IEEE Access
Multidisciplinary ⋮ Rapid Review ⋮ Open Access Journal

Received 7 November 2023, accepted 1 December 2023, date of publication 5 December 2023,
date of current version 13 December 2023.

Digital Object Identifier 10.1109/ACCESS.2023.3339844

RESEARCH ARTICLE

Radiated Emission Prediction of a BLDC Motor Using High-Frequency Simulations

JOOMIN PARK[1], (Student Member, IEEE), SONAPREETHA MOHAN RADHA[1], (Member, IEEE), SUNGJUN PARK[2], KYUNG-HUN JUNG[2], AND ICK-JAE YOON[1], (Senior Member, IEEE)

[1]Department of Electrical Engineering, Chungnam National University, Daejeon 34134, Republic of Korea
[2]Hanon System, Daejeon 34325, Republic of Korea

Corresponding author: Ick-Jae Yoon (ijyoon@cnu.ac.kr)

This work was supported by the Institute of Information and Communications Technology Planning and Evaluation (IITP) funded by the Korean Government (MSIT) through the Development of Advanced Power and Signal EMC Technologies for Hyper-Connected E-Vehicles under Grant 2020-0-00839.

ABSTRACT This paper presents a high-frequency model of a brushless DC motor to predict its radiated emission (RE) through high-frequency simulations of electromagnetic fields. The main RE noise path of the device-under-test (DUT) motor is specified as the stator winding, and its accurate high-frequency model in a full-wave EM simulator is proven by a two-port T-network. We analyze the induced surface current distribution according to the air ventilation hole shapes of the rotor housing and calculate the radiated electric field intensity using the high-frequency model of the DUT motor. The expected difference in the radiated electric field intensity by the hole configuration from the simulation model is verified experimentally.

INDEX TERMS Brushless DC motor, electromagnetic compatibility, high-frequency modeling, radiated emission.

I. INTRODUCTION

The electromagnetic compatibility (EMC) problems in electric motors and electronics of automobiles are getting increasingly noticed along with the rapid development of electric vehicles and self-driving technologies [1], [2], [3], [4]. They include violated conducted emission (CE) and radiated emission (RE) levels over the CISPR-25 regulations, mostly caused by the faster switching speed of the motor driver as well as the increased number of electric motors. The harmonic noise signals from the motor driver switching can be radiated through diverse paths of the motor: the noise current can flow along the power cable of the motor, and it eventually radiates via either the cable or the stator winding coils of the motor.

In the electrical device industry, the CE and RE noise tests for a device-under-test (DUT) are generally carried out before the final production. If the DUT fails to satisfy the regulations, it remains a burden to the companies because extra time and cost must be spent to resolve the problems. Against this background, efforts to predict the EMC features of the electric motors earlier in the design phase are ongoing. On printed circuit boards (PCBs), it was reported that the CE noise levels could be predicted by high-frequency circuit modeling of electronic components [5]. The RE noise level can be reduced in the design phase by signal integrity analysis, power integrity analysis, and trace layout of the PCBs [6], [7], [8]. However, they may not be suitable for predicting the RE noise trend or level of a three-dimensional (3D) electric motor unless its high-frequency modeling is present. Alternatively, the radiation mechanism from the winding coils of the electric motor can be expected from its impedance model, just like the radiation characteristic of the antenna can be inferred from its impedance behavior [9], [10], [11], [12]. It is worth noting that such impedance models can be readily calculated from full-wave electromagnetic (EM) simulations.

Fig. 1 shows the measured RE levels of a brushless DC (BLDC) motor under test in this work. (The measurement setup can be found from Fig. 12.) It is commonly believed that the radiated noise of a motor system mostly comes from

The associate editor coordinating the review of this manuscript and approving it for publication was Qinfen Lu.

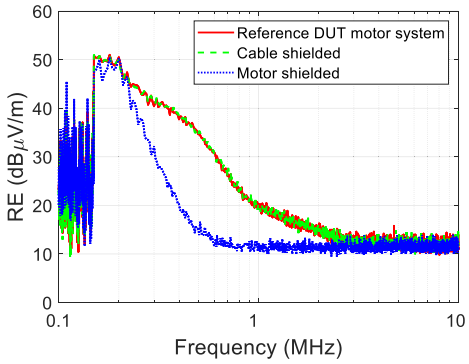

FIGURE 1. Measured radiated emissions of the DUT BLDC motor.

the cable harness. However, as can be seen from Fig. 1, the RE noise level does not change from that of the DUT motor system measurement even when the cable is shielded. The level rather decreases at 200 kHz–3 MHz frequencies when the motor itself is shielded, meaning that the main path of the RE noise is the motor, including the stator coil and rotor, not the cable for this DUT.

In this paper, we use a high-frequency modeling technique to predict the radiated electric field, mainly from the DUT motor using a full-wave EM simulator. To this end, we first build a high-frequency model of the stator winding in the Ansys HFSS and extract its impedance data of a single-phase operation considering the harmonic signal flow from the motor driver. Its accuracy is verified experimentally across a wide frequency range from 150 kHz to 30 MHz, wide enough to include the AM frequency (540 kHz – 1.7 MHz) band of interest from the motor industries. Consequently, we compare the radiated electric field level difference according to different configurations of the rotator housing's ventilation holes using the built high-frequency model. It is found that the difference in the radiated electric field intensity by the configuration of the holes can be estimated from the computed expectations, and such a comparison is further successfully verified through the measurement of the DUT motor prototypes in a semi-anechoic chamber.

II. HIGH-FREQUENCY MODELING

The main path of the radiated noise can be specified as the stator windings of the DUT from Fig. 1. Thus, it is essential to accurately identify its high-frequency impedance characteristics. In general, high-frequency modeling uses a high-frequency equivalent circuit, and it is indeed powerful in the prediction of CE noise from PCBs [13], [14], [15], [16]. However, in the case of RE noise, such a method is not such directive and could be less effective. This is because to include a highly accurate electrical characteristic model of a complex 3D configuration in an equivalent circuit is challenging. Instead, the impedance and radiation characteristics of the stator windings can be rather easily calculated using full-wave EM simulations, provided that the operating sequence of the motor is under consideration. Fig. 2a

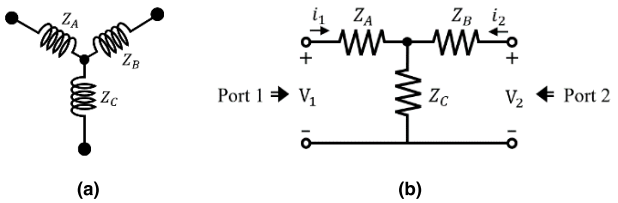

FIGURE 2. (a) Star-winding of the DUT motor. (b) Two-port T-network [14].

shows the star-wiring method of the DUT motor stator winding. Each inductor represents the total coil inductance of a single-phase operation. In the real model, each inductance is composed of four series multi-turn coils. The switching DC signal current from the motor inverter flows along the coil windings, or inductors. At the same time, the time harmonic signal generated by the inverter also flows along the windings where the EM field should radiate. This way, it acts as a radiator emitting RE noise. The radiated EM field eventually emits through the rotor housing body covering the stator coils, mainly by the air-vent holes of the rotor.

Fig. 2b shows the two-port T-network model [17], where each three-phase impedance of the stator winding is represented as Z_A, Z_B and Z_C. As is well known, the transfer impedance Z_{21} of the network is the same as Z_C, and the impedance for a single-phase inductance of the DUT motor can be calculated this way both in the full-wave EM simulation and measurement. The stator coil modeling and its measurement setup are shown in Fig. 3. We use HFSS from Ansys for all the full-wave simulations in this work. The material properties of the stator core and cover are given in Table 1. In Fig. 3a, a vertical metal bar connects each end of the winding of a single phase and the inverter PCB. The harmonic current from the PCB flows through the metal bar to the winding. Therefore, two rigid coaxial cables are also modeled and connected to the metal bars as shown in the figure such that the transfer impedance can be calculated. Each end of the coaxial cable is assigned with a wave port in the HFSS, to increase the accuracy of the simulation in the low frequency range. The same setup is made for the measurement as shown in Fig. 3b.

TABLE 1. Electrical material properties of the DUT motor stator parts.

Components	Material	Properties	Value
Stator core	Steel	Permeability	0.01 $[H/m]$
		Conductivity	0.38 $[\mu\Omega m]$
Stator cover	ABS	Relative Permittivity	2.8

Fig. 4 shows the simulated and measured impedance values according to the proposed setup. Note that only one case of the three-phase coils is plotted for brevity. It is observed that the two data agree very closely in the wide frequency range from 150 kHz to 30 MHz, meaning that the stator including the multi-turn coil winding is accurately set in Ansys HFSS.

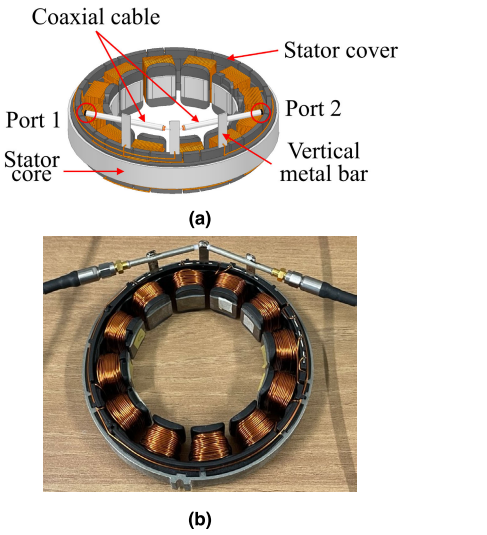

FIGURE 3. (a) Stator coil modeling in HFSS. (b) Impedance measurement setup.

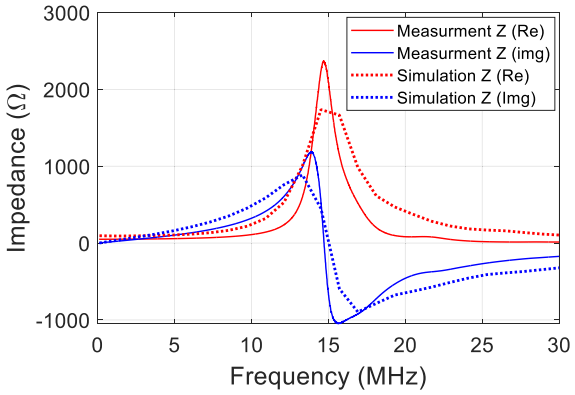

FIGURE 4. Simulated and measured impedance of the stator winding in the 150 kHz–30 MHz frequency range.

III. RADIATED FIELD ANALYSIS

Although it is always desired to predict the feasible EM noise characteristic including its change in level according to the DUT designs, such action is not easy to conduct in the DC motor design stage. It is again because its high-frequency modeling is usually not given. As it has been presented that the high-frequency impedance model can be appropriately set in the full-wave EM simulator, we now show its usage in predicting the radiated noise variation according to the rotor housing design of a reference DUT motor. Specifically, we show whether the relative difference in the radiated electric field level can be predicted from simulations.

A. APERTURE SHIELDING THEORY-BASED ROTOR HOUSING DESIGN

There must be air ventilation holes in the housing of motors as a means of preventing the deterioration of the motor from the heat generated by the windings and power electronics. The housing holes in Fig. 5 act as a radiating aperture

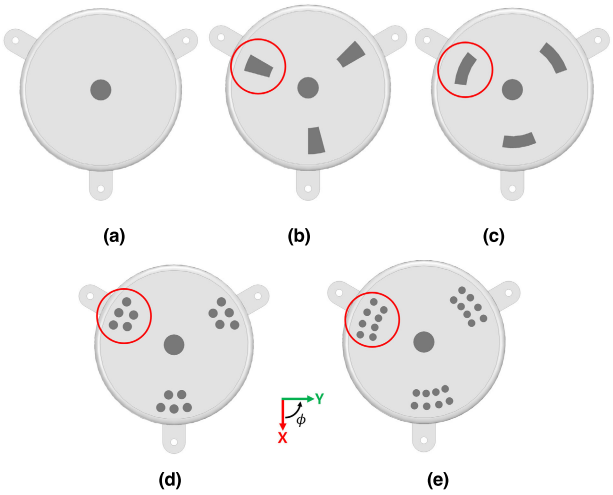

FIGURE 5. Housing model with different aperture configurations (D = maximum length of each aperture). (a) Without apertures. (b) $D = 24mm$ (reference model) (c) $D = 28mm$ (d) $D = 8.2\ mm$ (e) $D = 6.38\ mm$ (improved model).

of the electromagnetic field at the same time and should affect the shielding effectiveness. The magnetic field generated by the stator winding creates an induced current on the housing surface. The generated induced current creates a secondary magnetic field that forms an induced current in a direction canceling the original magnetic field on the surface of the housing. Therefore, the air ventilation holes on the housing create discontinuity with the induced currents. The diffracted induced currents cannot effectively cancel the original magnetic field, resulting in an increased radiated field level [18], [19], [20].

Fig. 5 shows the top views of the rotor housing of the DUT motor, with a variation in the ventilation hole (aperture) shapes. The common hole in the center of the housing is for motor shaft. The aperture under interest is marked with a solid circle. These models are set to compare the magnitude of the radiated electric field intensity according to the maximum length of the aperture of the housing. Note that the generated electric field from the stator coil inside the housing is along the ϕ-direction. Fig. 5b is the case of the reference aperture shape of the DUT whereas Fig. 5a is the case when all the holes are blocked. The total area of the holes is the same in Figs. 5b-5e. Fig. 6a shows the simulation setup for comparing the magnitude of the electric field emitted through the apertures. The electric field is measured at 1 meter in the z-direction, from the center of the motor. The simulated results are presented in Fig. 6b. It is first observed that Fig. 5a without any aperture shows the least electric field, confirming that the generated noise is mainly emitted through the aperture. Next, we can see that the magnitude of the electric field increases with the longer length of the aperture in ϕ.

Following to the previous study, Figs. 7a and 7b show the top views with the dimension of the rotor housings of Figs. 5b and 5e, respectively, on which the currents are induced from the stator coils inside in Fig. 7c. Following the rule of thumb

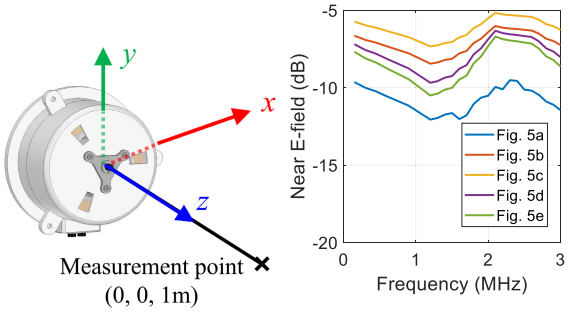

FIGURE 6. Electric field intensity comparison according to the aperture configurations. (a) Simulation setup for calculating the electric field intensity. (b) Simulation results.

in EMC design that the aperture should minimally interfere with the flow of the induced current, the shape of the single trapezoid hole in Fig. 7a is divided into a group of eight small circular holes with a diameter of 6.38 mm, as shown in Fig. 7b. Their total aperture area is 254.15 mm^2 close to that of a single trapezoid hole in Fig. 7a, which is 253.42 mm^2. We call the model in Fig. 7b the improved model from now on. Note that we assume that the difference in ventilation capability is negligible once the hole area is about the same. In addition, the shielding effect (S) according to the maximum length of the aperture L_{max} can be written as [18]:

$$S = 20\log\left[\frac{150}{f_{MHz}L_{max}}\right] \tag{1}$$

where f_{MHz} is the working frequency. For the case of multiple apertures, it is expressed as:

$$S = 20log\left[\frac{150}{f_{MHz}L_{max}\sqrt{n}}\right] \tag{2}$$

where n is the number of the apertures. According to (1) and (2), the ideal attenuation of the reference and improved model is calculated as 75.9 dB and 78.3 dB, respectively, showing 2.4 dB improvement in S.

According to the above two equations, the ideal attenuation of the reference model is 75.9 dB and the attenuation of the improved model is 78.3 dB. Changing from the single aperture of the reference model to the multiple aperture of the improved model thus increases S by approximately 2.4 dB, which is close to the difference in the emitted electric field between the cases of Figs. 5b and 5e, which is 2.1 dB.

B. INDUCED CURRENT ON THE ROTOR HOUSING

With the setup presented in Fig. 7, we plot the induced current distributions on the rotor housing at 1 MHz in Fig. 8 for the housing without aperture, with the trapezoid aperture (reference model) and with the circular hole aperture (improved model). The high-frequency model in Section II is utilized, and each port of for the three-phase stator coil is fed by a unit voltage with 120° phase difference (see Fig. 9a). It is observed in Fig. 8a that the induced currents flow in the ϕ-direction for the case without apertures, showing the desired

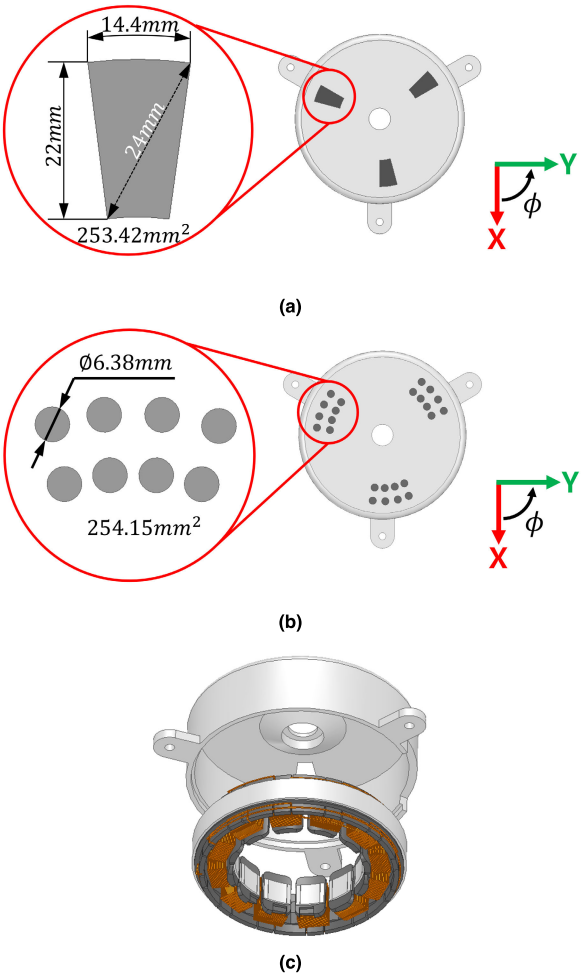

FIGURE 7. Rotor housing with air ventilation holes. (a) Reference model. (b) Improved model. (c) Housing with the stator coils.

current distribution for perfect shielding of the housing. The ventilation holes must be formed to avoid interfering with the flow of this induced current to achieve a good shielding effect.

Fig. 8b shows the induced current flow in the reference rotor housing. It is observed that the induced current is diffracted by the trapezoid aperture, as marked by a solid black arrow. On the other hand, we can clearly see that the induced current in the improved model in Fig. 8c flows through the holes, which is likely not the case in Fig. 8b, making the distribution more similar to Fig. 8a. One can expect that the radiated electric field level would be minimal for Fig. 8a, followed by the aperture configuration in Fig. 8c and Fig. 8b. This is the same order that was expected in Fig. 6b. Nevertheless, the similar current flow does not guarantee the same radiation level, as shown in Fig. 6b, because the noise still can be radiated through the apertures in the housing.

C. RADIATED EMISSION CHARACTERISTIC ANALYSIS

Consequently, we calculate the difference in the RE levels of the reference and improved housing models. The excitation setup of the stator coils is presented in Fig. 9a.

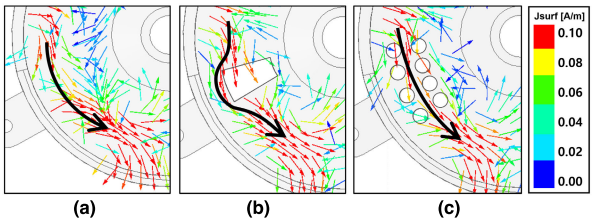

FIGURE 8. Induced current distribution of the rotor housing at 1 MHz. (a) Rotor housing without aperture. (b) Rotor housing with a trapezoid aperture. (c) Rotor housing with circular apertures.

The series coils in the same phase are marked with the same color of blue, green, and orange. Note that the end of each winding terminates at one side of the inner housing through a vertical bar, as represented in Fig. 3a. Each coil of the stator in the same phase is excited by a lumped port between the windings and the chassis ground, with $1V\angle 0°$ at port 1, $1V\angle 120°$ at port 2 and $1V\angle 240°$ at port 3. In addition, we model a rod monopole antenna operating from 100 kHz to 30 MHz to obtain the transmission coefficient between the DUT motor and the antenna as shown in Fig. 9b, by which the EM scattering behavior of the semi-anechoic chamber environment can be encountered. The antenna is terminated with a 50-Ω resistive load at port 4. The measurement table is also modeled. During the simulation, the five sides of the radiation box in Ansys HFSS but the ground are set to with perfect matched layers, instead of modeling the ferrite-based absorbers of an actual ALSE, which would require more computing power. The used setting is known to reduce the simulation time while providing an acceptable match between the simulation and measurement. Using the computing power of a 64-core CPU and 256 gigabytes of memory, the simulation took five hours to analyze about 800,000 meshed cells. More time and computing power will be needed to model accurate absorbers for the chamber environment, which remains another challenge [21], [22], [23].

Our RE simulation also includes the switching signal waveform feature of the driving motor driver because the radiated electric field should be proportional to the source intensity [18]. In other words, the electric field when radiated with the unit-voltage should be compensated with a practically used signal level. We measured the phase voltage between the port for each winding and the ground of the inverter in the time domain when the reference and the improved DUT motors are applied with a 280 V signal with a maximum rotational speed of 4,300 rpm. The switching waveforms at the maximum speed of the DUT are chosen because there is typically more emission at the maximum speed of the motor [24], [25], [26], [27]. The physical rotation of the rotor is not included since the RE difference would be negligible considering the observation frequency. The measurement points of the switching waveform at the inverter are described in Fig. 10a. Fig. 10b shows the schematic simulation diagram of the Ansys circuit for Fig. 9b.

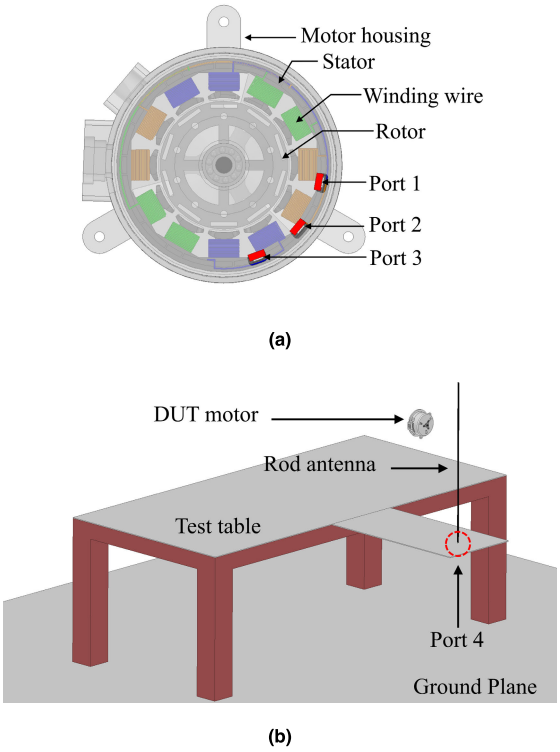

FIGURE 9. Radiated electric field simulation setup. (a) Simulation model. (b) Measurement environment modeling according to the CISPR-25 standard.

The computed transmission coefficients between each phase of the stator winding and antenna obtained from the full-wave EM simulation setup in Fig. 10b are inserted into the circuit simulator as a black box and noted as an EM component in Fig. 10b. Simultaneously, the measured switching waveforms of each phase of the stator winding are addressed to each phase port of the EM component through a circuit simulator. The switching waveform, as an input, is converted to the antenna port through the EM component, which induces a voltage at the 50-Ω resistive load of the antenna. The voltage in the time domain induced by the resistive load is transformed into the frequency domain through a Fourier transform. The antenna voltage obtained this way is finally converted into an electric field radiated from the DUT motor, by multiplying it with the antenna factor of the rod antenna.

In Fig. 13. the final simulation results of the RE of the motors are shown in yellow and purple solid lines. As expected, we see that the radiated electric field decreases w0ith the improved hole design compared with the reference model by 0.8 to 3.2 dB in the frequency range between 150 kHz and 3 MHz, showing that the RE level change of an electric motor can be estimated using high-frequency simulations.

IV. RADIATED EMISSION MEASUREMENT

Measurements were carried out under CISPR-25 regulations to verify the electric field level difference of the motors

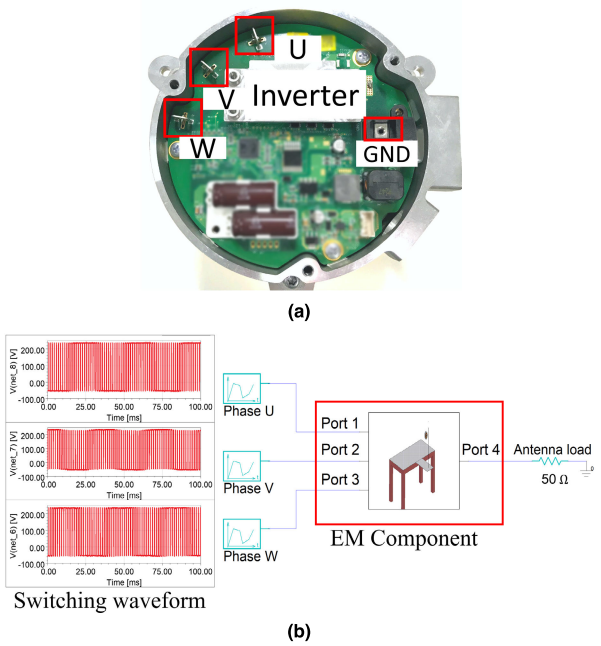

FIGURE 10. Switching waveform measurement and circuit simulation set up. (a) Switching waveform measurement points. (b) Circuit simulation schematic.

FIGURE 11. Built prototypes. (a) DUT motor with reference trapezoid apertures. (b) DUT motor with improved circular hole apertures.

expected from the simulations. The motor prototypes are built as shown in the photos in Fig. 11. Note that only the housing aperture configuration is different, whereas all the other parts and operating conditions are the same.

Fig. 12 shows the measurement setup in an absorber-lined shielded enclosure (ALSE) in accordance with CISPR-25 regulations [28]. Although the power cable to the DUT is shielded, it still could form a common mode loop for the common mode radiation. To exclude any influence from the cable during the measurement, the possible RE of the cable was measured by shielding the DUT under operation with a metal box as shown in Fig. 12b. The RE level from the DUT alone but still under operation can be obtained as red and blue solid lines in Fig. 13 by subtracting the measured radiation level of the other components but DUT of Fig. 12b from the measured radiation intensity of the unshielded DUT of Fig. 12a.

First, we see that the improved model shows less emission than the reference model by 0.8 to 3.5 dB in the 150 kHz–3

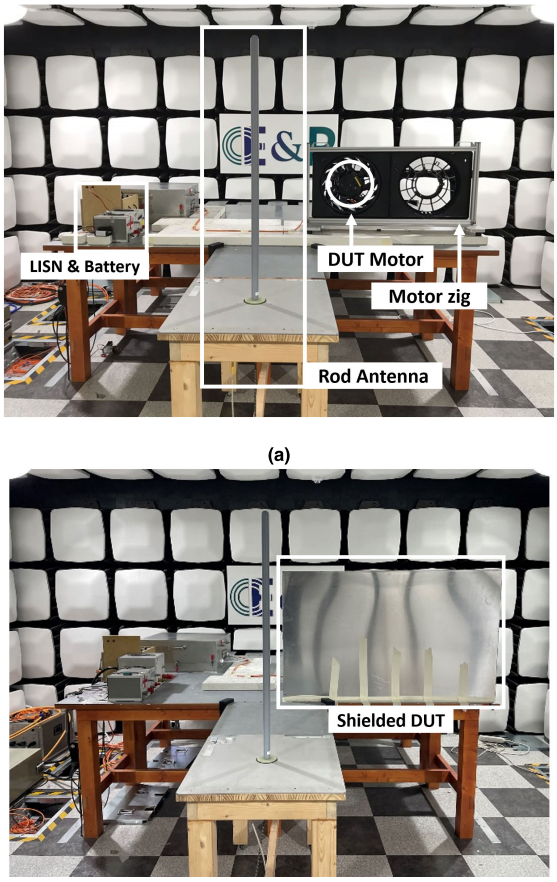

FIGURE 12. Photos of the measurement setup in an absorber-lined shielded enclosure in accordance with CISPR-25 regulations. (a) DUT measurement. (b) Shielded DUT measurement.

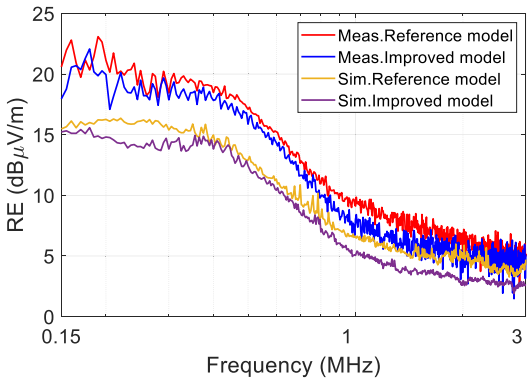

FIGURE 13. Comparison of the radiated emission between the simulation and measurement.

MHz frequency range, very close to the relative difference from the simulation. In both results of the simulation and measurement, we also observe that the absolute RE level of the improved model is reduced over the frequencies. There is maximally 6.49 dB at 190 kHz difference between the simulations and measurements. This might be because the current simulation setup does not include the EM influence

from the motor zig and chamber absorbers which also could cause additional scattering in the radiated electric field from the DUT. A perfect chamber absorber modeling would further minimize the gap between the simulation and measurement, although a perfect matching between the simulation and measurement in 3D simulations remains a challenge [24], [25], [26]. Nevertheless, our results show a deviation of 3-4.2 dB in the AM band, with a high similarity in decaying tendency of the field intensity across the frequency. Moreover, the overall relative difference in the radiated field intensity from the difference in the 3D configuration can be successfully estimated [29], [30].

V. CONCLUSION

In this paper, we showed that highly accurate high-frequency modeling of a complex DC motor stator winding can be appropriately set in a full-wave EM simulator, and it can be effectively used in predicting the RE differences from the variations in the 3D rotor housing configuration. The simulation successfully predicts the overall ups and downs of the field variation according to the configurations of the air ventilation holes, with a deviation in the absolute field intensity level of about 3-4.2 dB in the AM band. The inclusion of the missed EM field behavior of the motor zig and chamber absorber would make the proposed simulation setup more rigorous, and this remains as a future work. Nevertheless, the reported high-frequency design technique of the motor in this work is expected to be useful for static field motor designs operating under EMC regulations as it shows the possibilities of expecting the overall variations of the radiated noise according to the configurations of the motor.

REFERENCES

[1] H. Hirsch, S. Jeschke, L. Wei, M. Trautmann, J. Bärenfänger, M. Maarleveld, J. Heyen, and A. Darrat, "Latest development of the national and international EMC-standards for electric vehicles and their charging infrastructure," in *Proc. IEEE Int. Symp. Electromagn. Compat. (EMC)*, Aug. 2015, pp. 708–713.

[2] T. Campi, S. Cruciani, V. De Santis, F. Maradei, and M. Feliziani, "EMC and EMF safety issues in wireless charging system for an electric vehicle (EV)," in *Proc. Int. Conf. Electr. Electron. Technol. Automot.*, Jun. 2017, pp. 1–4.

[3] V. M. Ionescu, A.-A. Sapunaru, C. L. Popescu, and M. O. Popescu, "EMC normes for testing electric and hybrid cars," in *Proc. Electr. Vehicles Int. Conf. (EV)*, Oct. 2019, pp. 1–4.

[4] N. A. Enegbuma and S. Kim, "Analyzing DC and AC magnetic field intensity, distribution, and relationship in a Hyundai IONIQ 2016 electric vehicle," *J. Electromagn. Eng. Sci.*, vol. 21, no. 4, pp. 282–290, Sep. 2021.

[5] L. Zhai and C. Song, "Conducted EMI from motor drive system of electric vehicle under load operation," in *Proc. Asia–Pacific Int. Symp. Electromagn. Compat. (APEMC)*, Jun. 2017, pp. 181–183.

[6] D. Moongilan, "Image and return current modeling of PCB traces for radiated emissions," in *Proc. IEEE EMC Int. Symp., Symp. Rec., Int. Symp. Electromagn. Compat.*, Mar. 2001, p. 927.

[7] J. Yao, S. Wang, and Z. Luo, "Near field coupling's impact on radiated EMI and mitigation techniques for power converters in automotive applications," in *Proc. IEEE Energy Convers. Congr. Expo. (ECCE)*, Feb. 2020, pp. 5882–5889.

[8] S. Heidari, M. Mehri, and N. Masoumi, "System level estimation of a PCB electromagnetic radiated emission," in *Proc. IEEE 20th Workshop Signal Power Integrity (SPI)*, Turin, Italy, May 2016, pp. 1–4.

[9] J. Yao, Y. Li, S. Wang, X. Huang, and X. Lyu, "Analysis and reduction of radiated EMI in high-frequency GaN IC-based active clamp flyback converters," in *Proc. IEEE Appl. Power Electron. Conf. Exposit. (APEC)*, New Orleans, LA, USA, Mar. 2020, pp. 664–671.

[10] J. Lee, K. Jung, and S. Park, "Simulation of radiated emissions from a low voltage BLDC motor," in *Proc. Int. Symp. Antennas Propag. (ISAP)*, Busan, South Korea, Oct. 2018, pp. 1–2.

[11] C. A. Balanis, *Antenna Theory: Analysis and Design*, 4th ed. Hoboken, NJ, USA: Wiley, 2016, pp. 173–180.

[12] Y. Zhang, S. Wang, and Y. Chu, "Modeling and reduction of radiated EMI for isolated power converters," in *Proc. IEEE Appl. Power Electron. Conf. Expo. (APEC)*, Mar. 2018, pp. 1778–1785.

[13] Y. Ryu, M. Yea, J. Kim, and K. J. Han, "Stator impedance modeling platform for the electromagnetic compatibility aware design of 3.7- to 7.5-KW squirrel-cage induction motors," *IEEE Trans. Ind. Electron.*, vol. 68, no. 11, pp. 11255–11265, Nov. 2021.

[14] G. Almandoz, S. Zarate, A. Egea, Y. Moreno, A. Urdangarin, and R. Moreno, "High frequency modeling of electric drives for electromagnetic compatibility analysis," in *Proc. Int. Conf. Electr. Mach. (ICEM)*, vol. 1, Aug. 2020, pp. 1129–1135.

[15] Y. Ryu and K. J. Han, "Extraction of high-frequency phase-to-phase coupling in AC machine using mixed-mode network parameters," *IEEE Trans. Magn.*, vol. 52, no. 3, pp. 1–4, Mar. 2016.

[16] T.-Y. Kim and J.-H. Lee, "A simple power source modeling and experimental investigation of a spacecraft for EMC applications," *J. Electromagn. Eng. Sci.*, vol. 21, no. 1, pp. 78–85, Jan. 2021.

[17] D. M. Pozar, *Microwave Engineering*, 4th ed. Hoboken, NJ, USA: Wiley, 2011, pp. 190–192.

[18] H. W. Ott, *Electromagnetic Compatibility Engineering*, Hoboken, NJ, USA: Wiley, 2009, pp. 267–273.

[19] F. A. Po'ad, M. Z. M. Jenu, C. Christopoulos, and D. W. P. Thomas, "Estimation of electric and magnetic shielding effectiveness of a metallic enclosure with apertures," in *Proc. Int. RF Microw. Conf.*, Putra Jaya, Malaysia, Sep. 2006, pp. 291–295.

[20] P. Dehkhoda, A. Tavakoli, and R. Moini, "An efficient and reliable shielding effectiveness evaluation of a rectangular enclosure with numerous apertures," *IEEE Trans. Electromagn. Compat.*, vol. 50, no. 1, pp. 208–212, Feb. 2008.

[21] F. Lafon, R. Dupendant, and J. Davalan, "Invesigation on dispersions between CISPR25 chambers for radiated emissions below 100 MHz," in *Proc. Int. Symp. Electromagn. Compat.*, Sep. 2014, pp. 29–34.

[22] F. Lafon, J. Davalan, and R. Dupendant, "Inter-laboratory comparison between CISPR25 chambers, identification of influent parameters and analysis by 3D simulation," in *Proc. Asia–Pacific Symp. Electromagn. Compat. (APEMC)*, May 2015, pp. 71–74.

[23] F. Lafon, R. Dupendant, J. Davalan, and C. Chevriau, "Identification and study of influential parameters in CISPR25 radiated emissions test setup by interlaboratory measurements and 3-D simulation combined analysis," *IEEE Trans. Electromagn. Compat.*, vol. 58, no. 5, pp. 1398–1406, Oct. 2016.

[24] S. Wei, Z. Pan, J. Yang, and P. Du, "A fast prediction approach of radiated emissions from closely-spaced bent cables in motor driving system," *IEEE Trans. Veh. Technol.*, vol. 71, no. 6, pp. 6100–6109, Jun. 2022.

[25] I. Oganezova, R. Kado, B. Khvitia, A. Gheonjian, and R. Jobava, "Simulation of conductive and radiated emissions from a wiper motor according to CISPR 25 standard," in *Proc. IEEE Int. Symp. Electromagn. Compat. (EMC)*, Aug. 2015, pp. 963–968.

[26] S. Wei, Z. Pan, J. Fan, and P. Du, "Prediction of radiated EMI from permanent magnet synchronous motor based on field-circuit coupled method," in *Proc. World Congr. Eng.*, 2019, pp. 433–437.

[27] I. Oganezova, R. Kado, B. Khvitia, Z. Kuchadze, A. Gheonjian, and R. Jobava, "EMC model of low voltage DC motor," in *Proc. IEEE Int. Symp. Electromagn. Compat. (EMC)*, Raleigh, NC, USA, Aug. 2014, pp. 81–85.

[28] *Vehicles, Boats and Internal Combustion Engines-Radio Disturbance characteristic-Limits and Methods of Measurements for the Protection of on-Board Receivers*, CISPR, 2016.

[29] C. Ma and H. Cao, "Simulation and analysis of a shielding cavity used in on-site radiated emission measurement," in *Proc. 7th IEEE Int. Symp. Microw., Antenna, Propag., EMC Technol. (MAPE)*, Oct. 2017, pp. 206–208.

[30] N. Sood, "Validation of anechoic chamber for radiated emission test," in *Proc. 15th Int. Conf. Electromagn. Interference Compat. (INCEMIC)*, Nov. 2018, pp. 1–4.

JOOMIN PARK (Student Member, IEEE) received the B.S. degree in radio science and engineering from Kongju National University, Cheonan, Republic of Korea, in 2016, and the M.S. degree in electrical engineering from Chungnam National University (CNU), Daejeon, South Korea, in 2021, where he is currently pursuing the Ph.D. degree in electrical engineering. His research interests include electromagnetic compatibility, high-frequency modeling, and EMC design for E-vehicle electric motors.

SONAPREETHA MOHAN RADHA (Member, IEEE) received the B.S. degree in electronics and communication engineering from Anna University, Chennai, India, in 2012, the M.S. degree in nuclear and quantum engineering from the Korea Advanced Institute of Science and Technology (KAIST), Daejeon, Republic of Korea, in 2016, and the Ph.D. degree in electrical engineering from Chungnam National University (CNU), Daejeon, in 2022. She is currently a Postdoctoral Researcher with the Radio and Electrical Engineering Research Institute, CNU. Her research interests include electrically small antennas, electromagnetic compatibility, metamaterials, and wireless power transfer.

SUNGJUN PARK received the B.S. degree in electrical engineering from Seoul National University, Seoul, Republic of Korea, in 2011. He has been with Hanon Systems Company, Daejeon, Republic of Korea, since 2011. His research interests include power electronics circuit and its electromagnetic compatibility design optimization.

KYUNG-HUN JUNG received the B.S. and M.S. degrees in mechanical engineering from Chonnam National University, Gwangju, Republic of Korea, in 2000 and 2002, respectively, and the Ph.D. degree in electrical engineering from Chungnam National University, Daejeon, Republic of Korea, in 2018. He has been with Hanon Systems Company, Daejeon, since 2008. His research interests include electric motor design and analysis.

ICK-JAE YOON (Senior Member, IEEE) received the B.S. and M.S. degrees in electrical engineering from Yonsei University, Seoul, Republic of Korea, in 2003 and 2005, respectively, and the Ph.D. degree in electrical engineering from The University of Texas, Austin, TX, USA, in 2012.

He joined as a Faculty Member of Chungnam National University, Daejeon, Republic of Korea, in 2014, where he is currently a Professor with the Department of Electrical Engineering. From 2012 to 2014, he was with the Electromagnetic Systems Group, Electrical Engineering Department, Technical University of Denmark (DTU), Lyngby, Denmark, as a Postdoctoral Research Fellow and an Assistant Professor. From 2005 to 2008, he was a Research Engineer with the Samsung Advanced Institute of Technology, Samsung Electronics Company, Yongin, Republic of Korea. His current research interests include antennas, RF/microwave circuits, electromagnetic compatibility, and theoretical methods for electromagnetics. He received the H. C. Ørsted Postdoctoral Fellowship from DTU, in 2012. He has been an Associate Editor for the *IEICE Transactions on Communications*, since 2019.